

SPAD-Based Optical Wireless Communication with Signal Pre-Distortion and Noise Normalization

Shenjie Huang and Majid Safari

Abstract

In recent years, there has been a growing interest in exploring the application of single-photon avalanche diode (SPAD) in optical wireless communication (OWC). As a photon counting detector, SPAD can provide much higher sensitivity compared to the other commonly used photodetectors. However, SPAD-based receivers suffer from significant dead-time-induced non-linear distortion and signal dependent noise. In this work, we propose a novel SPAD-based OWC system in which the non-linear distortion caused by dead time can be successfully eliminated by the pre-distortion of the signal at the transmitter. In addition, another system with joint pre-distortion and noise normalization functionality is proposed. Thanks to the additional noise normalization process, for the transformed signal at the receiver, the originally signal dependent noise becomes signal independent so that the conventional signal detection techniques designed for AWGN channels can be employed to decode the signal. Our numerical results demonstrate the superiority of the proposed systems compared to the state-of-the-art systems in terms of BER performance and achievable data rate.

Index Terms

Optical wireless communication, single photon avalanche diode, noise normalization.

I. INTRODUCTION

In recent years, there is an increase of interest in employing the single photon avalanche diode (SPAD) in optical wireless communications (OWC) [1]–[4]. To achieve a SPAD receiver, the

The authors are with the School of Engineering, the University of Edinburgh, Edinburgh EH9 3JL, U.K. (e-mail: {shenjie.huang, majid.safari}@ed.ac.uk).

commonly used photodiode should be biased above the breakdown voltage so that it operates in the so-called Geiger mode. One of the main advantages of the SPAD lies in its high sensitivity compared to the other commonly used photodetectors such as PIN photodiode and avalanche photodiode (APD). As summarized in [5], the SPAD-based receivers can achieve sensitivity distance to the quantum limit down to only 12 dB; however, for APD-based receivers the corresponding distance is around 20 dB. In the literature, the application of SPAD receivers in visible light communication (VLC) has been widely investigated [1], [6]–[8]. For instance, by using the off-the-shelf SPAD receiver, an achievable data rate of more than 2 Gbps with BER of 10^{-3} is demonstrated in [8]. Some other works also investigate the application of SPAD-based receivers in underwater wireless optical communication (UWOC) [3], [9], free-space optical communication (FSO) [10], and vehicular optical communication [11].

Although SPAD-based receiver can provide excellent single photon sensitivity and picosecond temporal resolution, it suffers from some non-ideal effects such as dead time, crosstalk and afterpulsing. In particular, dead time can introduce significant communication performance degradation which needs to be carefully addressed. Dead time refers to the short time period of several nanoseconds after each triggered avalanche when the SPAD is getting quenched and hence is unable to detect photons [9]. Based on different employed quenching circuits, SPAD is usually classified into two main types, i.e., active quenching (AQ) and passive quenching (PQ) SPAD. For AQ SPADs the dead time remains constant, but for PQ SPADs, due to the paralysis property, the photon arrivals during the dead time can extend its duration [12]. To improve the performance of SPAD-based receivers in the presence of dead time, a novel detection scheme by utilizing not only the photon count information but also the photon arrival information is proposed in [4]. In addition, the SPAD receiver with variable optical attenuator which can adaptively control the incident photon rate of the SPAD array is investigated in [10]. However, all these techniques require additional hardware at the receiver which inevitably increases the complexity of the receiver design. Therefore, it is crucial to propose cost-effective signal processing techniques for SPAD-based systems to realize performance improvement without any additional hardware requirements.

Some works in the literature have investigated the signal processing techniques to enhance the performance of OWC systems with signal-dependent noise whose power is proportional to the amplitude of the received signal [13], [14]. In [13], the signalling in the square-root

domain is proposed which can transform the signal-dependent noise into signal-independent one to simplify the decoding process and improve the BER performance. Such transformation has been further applied to SPAD-based OWC systems [9] and optical fibre communication [15]–[17]. In addition, in [14] an improved constellation and decoding threshold design for such signal dependent channel is obtained by solving the optimization problem aiming at minimizing the error probabilities. However, due to the presence of dead time, the signal-dependent noise effect of SPAD receivers is much more complicated than the one described above [18]. As a result, employing the aforementioned techniques directly in SPAD-based systems cannot achieve the optimal performance. Furthermore, besides the distinct signal-dependent noise, the dead time of SPAD also introduces an additional non-linear signal distortion which makes the channel model different from the simple linear channel model considered in the above works. Therefore, some novel signal processing techniques designed based on the unique properties of SPAD should be proposed to enhance the performance of SPAD-based systems.

In this work, we propose two novel SPAD-based systems to mitigate the dead time effects using signal processing techniques. The first is the system with pre-distortion in which the non-linear distortion caused by dead time can be eliminated through the pre-distortion of the signal at the transmitter. The second is the system with joint pre-distortion and noise normalization functionality. In this system, besides the pre-distortion functionality, the employed noise normalization process can transfer the original signal dependent noise into signal independent one so that the conventional signal detection techniques designed for AWGN channels can be easily employed to decode the received signal. The latter system outperforms the former one; whereas, the advantage of the former system lies in its simplicity. To the best of authors' knowledge, the SPAD-based systems with the above functionalities have not been investigated before. Through our extensive numerical results, it is demonstrated that the proposed systems can achieve much better BER and achievable data rate performance compared to the state-of-the-art systems.

The rest of this paper is organized as follows. Section II introduces channel model of the SPAD-based OWC systems and the performance of the two state-of-the-art systems, i.e., system with uniform signalling and square-root transform. Section III presents the proposed two SPAD-based systems, i.e., system with pre-distortion and system with joint pre-distortion and noise normalization, and the corresponding BER expressions are derived. Later, the numerical results and discussion are presented in Section IV. Finally, we conclude this paper in Section V.

II. SPAD-BASED OWC SYSTEMS

A. Channel Model

We consider that single-carrier pulse amplitude modulation (PAM) scheme is employed in the considered SPAD-based OWC systems, although the proposed idea in this work can also be extended to systems with other modulation schemes, e.g., OFDM. The transmitted M -ary PAM message vector can be expressed as

$$\mathbf{s} = [0, 1, 2, \dots, (M-1)]^T. \quad (1)$$

Assuming that after mapping the corresponding vector of the transmitted photon rates is given by

$$I(\mathbf{s}) = [I(0), I(1), I(2), \dots, I(M-1)]^T, \quad (2)$$

the average transmitted optical power can be expressed as

$$P_T = h\nu E[I(\mathbf{s})] = \frac{h\nu}{M} \sum_{m=0}^{M-1} I(m), \quad (3)$$

where $h\nu$ is the photon energy. Considering that the path loss introduced by the channel is α , the average received signal power can be written as

$$P_R = \alpha P_T = \frac{\alpha h\nu}{M} \sum_{m=0}^{M-1} I(m). \quad (4)$$

In order to achieve higher data rates and additional protection against the background light, SPAD-based receivers in OWC systems are usually implemented in arrays [7]–[9]. When the m th symbol is transmitted at the transmitter, the received photon rate for each SPAD in the array is given by

$$\lambda_m = \frac{\Upsilon (P_{R,m} + P_b)}{Nh\nu} = \frac{\Upsilon [\alpha I(m) + \lambda_{b,\text{tot}}]}{N}, \quad (5)$$

where Υ is the SPAD photon detection efficiency (PDE), $P_{R,m}$ denotes the received optical power when the m th symbol is transmitted, P_b refers to the total received background power, N denotes the number of SPAD pixels in the array receiver, and $\lambda_{b,\text{tot}} = P_b/h\nu$ is the total received background photon rate. Considering that the employed SPAD receiver is PQ-based, when the received signal is with photon rate of λ_m , the output photocount distribution of each

SPAD pixel can be approximated as sub-Poisson distribution with mean [19]–[21]

$$\mu_{m,\text{single}} = \lambda_m T_s e^{-\lambda_m T_d}, \quad (6)$$

and variance [19], [22]

$$\sigma_{m,\text{single}}^2 = \begin{cases} \mu_{m,\text{single}} - \mu_{m,\text{single}}^2, & T_s \leq T_d, \\ \mu_{m,\text{single}} - \mu_{m,\text{single}}^2 \left[1 - \left(1 - \frac{T_d}{T_s} \right)^2 \right], & T_s > T_d, \end{cases} \quad (7)$$

where T_s and T_d represent the symbol duration and dead time, respectively. Since the variance of the photocount is less than its mean, the above distribution shows the sub-Poisson characteristics. Note that compared to AQ SPAD, PQ SPAD benefits from its simpler circuit design and higher PDE and is widely employed in the commercial SPAD receivers [23]. In this work, we hence consider that the SPAD is PQ-based. Equation (6) presents that dead time results in the paralysis property of the PQ SPAD and introduces the non-linear distortion to the received signal. In addition, it is demonstrated in (7) that the noise variance of the SPAD output is signal dependent. Note that this signal dependent noise is different from the traditional one investigated in the literature whose power is proportional to the signal amplitude [13], [14]. For a SPAD array detector with sufficient large number of pixels, based on the central limit theorem, the total output photocount can be approximated as Gaussian distributed random variable with mean

$$\mu_m = N\mu_{m,\text{single}}, \quad (8)$$

and variance

$$\sigma_m^2 = N\sigma_{m,\text{single}}^2. \quad (9)$$

To make a fair comparison among the different systems considered in this work, we employ three constraints on the transmitted photon rates (2). Due to the considered intensity modulation direct detection (IM/DD) modulation, the photon rate $I(m)$ should be non-negative. To satisfy this requirement and ensure that the largest dynamic range is utilized, the first constraint is given by

$$I(0) = 0. \quad (10)$$

The second constraint is the average power constraint that $P_T \leq P_{\text{ave}}$ where P_{ave} denotes the

average power limit of the transmitter. Invoking the expression of P_T given in (3), this constraint can be expressed as

$$\frac{h\nu}{M} \sum_{m=0}^{M-1} I(m) \leq P_{\text{ave}}. \quad (11)$$

The third considered constraint is the peak power constraint aiming to avoid the strong SPAD nonlinear distortion. As illustrated in (6), due to the presence of dead time, with the increase of the received photon rate the detected average photon count firstly increases and then decreases. The received photon rate which gives the highest detected photon count, also known as the saturation point, is given by $1/T_d$ [10]. A peak received power constraint can be put to limit the received photon rate below this saturation point, i.e.,

$$\lambda_{M-1} \leq \frac{1}{T_d}. \quad (12)$$

Invoking the relationship between the transmitted and received photon rates given in (5), (12) can be rewritten as the constraint on the peak transmitted photon rate

$$I(M-1) \leq \frac{N}{\alpha T_d \Upsilon} - \frac{\lambda_{b,\text{tot}}}{\alpha}. \quad (13)$$

B. System with Uniform Signalling

The system with uniform signalling is the simplest and the most common one [13]. In such system, the transmitted photon rates are uniformly spaced which can be expressed as

$$I_{\text{uni}}(\mathbf{s}) = [0, d, 2d, \dots, (M-1)d]^T, \quad (14)$$

where d refers to the constellation level separation at the transmitter. To make sure that the average transmitted power constraint (11) is satisfied, the limitation of d is can be expressed as

$$d \leq \frac{2P_{\text{ave}}}{h\nu(M-1)}. \quad (15)$$

In addition, the peak power constraint given in (13) can be rewritten as

$$d \leq \frac{1}{M-1} \left[\frac{N}{\alpha T_d \Upsilon} - \frac{\lambda_{b,\text{tot}}}{\alpha} \right]. \quad (16)$$

$$\delta_m = \frac{\frac{\mu_m}{\sigma_m^2} - \frac{\mu_{m+1}}{\sigma_{m+1}^2} + \sqrt{\left(\frac{\mu_m}{\sigma_m^2} - \frac{\mu_{m+1}}{\sigma_{m+1}^2}\right)^2 - \left(\frac{1}{\sigma_m^2} - \frac{1}{\sigma_{m+1}^2}\right) \left\{ \left(\frac{\mu_m^2}{\sigma_m^2} - \frac{\mu_{m+1}^2}{\sigma_{m+1}^2}\right) + 2 \ln \left(\frac{\sigma_m}{\sigma_{m+1}}\right) \right\}}{\frac{1}{\sigma_m^2} - \frac{1}{\sigma_{m+1}^2}}. \quad (20)$$

In order to achieve the best BER performance and ensure that the above constraints are all satisfied, the optimal d is given by

$$d_{\text{uni}}^* = \min \left\{ \frac{2P_{\text{ave}}}{h\nu(M-1)}, \frac{1}{M-1} \left[\frac{N}{\alpha T_d \Upsilon} - \frac{\lambda_{b,\text{tot}}}{\alpha} \right] \right\}. \quad (17)$$

At the receiver, the corresponding received photon rate for each SPAD pixel when the m th symbol is transmitted can be written as

$$\lambda_{\text{uni},m} = \frac{\Upsilon [\alpha m d_{\text{uni}}^* + \lambda_{b,\text{tot}}]}{N}. \quad (18)$$

By substituting (18) into (8) and (9), the mean and variance of the SPAD output signal can be achieved. Since in the considered system the received constellation levels are not equally space and the noise variance is signal dependent, the commonly used BER expression for PAM-based AWGN channel cannot be employed. Based on the maximum likelihood (ML) rule, the accurate BER for such system can be expressed as [13]

$$P_{\text{eb}} = \frac{1}{M \log_2(M)} \sum_{m=1}^{M-1} Q \left(\frac{\delta_m - \mu_m}{\sigma_m} \right) + Q \left(\frac{\mu_{m+1} - \delta_m}{\sigma_{m+1}} \right), \quad (19)$$

where δ_m with $0 \leq m \leq M-1$ denotes the optimal thresholds calculated based on the moments μ_m and σ_m^2 which are given by (20).

C. System with Square-Root Transform

The square-root transform (SQRT) has been applied to the general OWC systems [9], [13], [14] and fibre optical communication systems [15], [17]. In this section, we will briefly introduce the SPAD-based system with SQRT.

For system with SQRT, a square-root operation is applied to the received signal and at the transmitter an inverse transform, i.e., square operation, is employed. Therefore, the transmitted

photon rate vector can be expressed as

$$I_{\text{sqrt}}(\mathbf{s}) = [0, d, 4d, \dots, (M-1)^2 d]^T. \quad (21)$$

Note that different from the photon rates given in (14), here the transmitted photon rates are not equally spaced. Now let's consider the optimal selection of d in this system. With the considered photon rate transmission, the average transmitted power constraint (11) can be rewritten as

$$d \leq \frac{6P_{\text{ave}}}{h\nu(M-1)(2M-1)}. \quad (22)$$

Furthermore, the peak power constraint introduced by the SPAD receiver nonlinearity (13) results in

$$d \leq \frac{1}{(M-1)^2} \left[\frac{N}{\alpha T_d \Upsilon} - \frac{\lambda_{b,\text{tot}}}{\alpha} \right]. \quad (23)$$

Therefore, the optimal value of d is given by

$$d_{\text{sqrt}}^* = \min \left\{ \frac{6P_{\text{ave}}}{h\nu(M-1)(2M-1)}, \frac{1}{(M-1)^2} \left[\frac{N}{\alpha T_d \Upsilon} - \frac{\lambda_{b,\text{tot}}}{\alpha} \right] \right\}. \quad (24)$$

By substituting d_{sqrt}^* into (21), the designed transmitted photon rate can be determined. Invoking (5) the corresponding received photon rate for each SPAD can be expressed as

$$\lambda_{\text{sqrt},m} = \frac{\Upsilon [\alpha m^2 d_{\text{sqrt}}^* + \lambda_{b,\text{tot}}]}{N}. \quad (25)$$

After taking the square-root transform at the receiver, the mean of the transformed signal can be approximated as

$$\mu_{\text{sqrt},m} = \sqrt{N \lambda_{\text{sqrt},m} T_s} e^{-\frac{1}{2} \lambda_{\text{sqrt},m} T_d}. \quad (26)$$

When the noise variance has linear relationship with the signal amplitude, the system with SQRT can achieve the equidistant transformed received signal with normalized noise variance [13]. However, since the relationship between the noise variance and signal amplitude of the SPAD output (as shown in (7)) is not linear, SPAD-based system with SQRT cannot achieve the optimal performance. As a result, as shown in (26) the transformed PAM signal is not equidistant. In addition, the noise variance of the transformed signal still keeps its signal dependency. Therefore, (19) should again be employed to evaluate the BER performance of the considered system. Note that although the mean of the transformed signal is given by (26), the expression of its variance

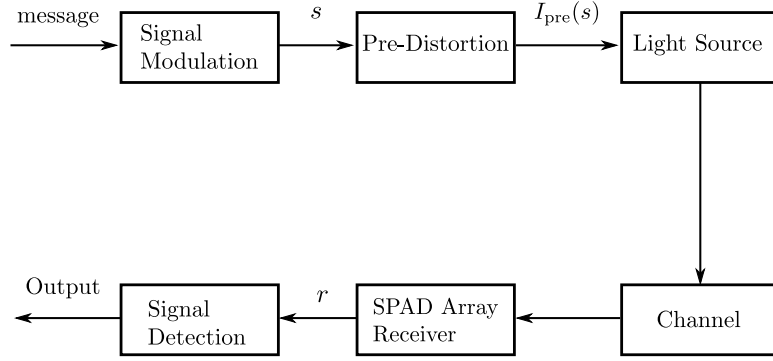


Fig. 1. The schematic of the proposed SPAD-based OWC system with signal pre-distortion.

is analytically intractable. In order to achieve the decoding threshold (20), the variance of the transformed signal should be calculated numerically through the simulation.

III. THE PROPOSED SYSTEMS

The performance of the state-of-the-art SPAD-based OWC systems introduced in Section II is strongly degraded by the dead time effects. In this section, we propose two novel systems aiming to mitigate the dead time effects and improve the communication performance.

A. System with Pre-Distortion

The schematic of the first proposed SPAD-based system is shown in Fig. 1. At the transmitter of the proposed system, a pre-distortion process is applied to the generated PAM signal and the output signal is then fed to the light source. After propagating through the free-space channel, the optical signal is received by the SPAD array at the receiver. The employed pre-distortion process is designed to compensate the non-linear distortion of the SPAD output induced by the dead time and realize the equidistant received signal. Note that similar signal pre-distortion idea has been proposed in VLC systems to compensate the nonlinearity effects introduced by LEDs [24]. However, to the best of the authors' knowledge, its application in SPAD-based systems to combat the dead time effects has not been investigated before. In this section, we will fill this research gap.

Invoking (5) and (8), the relationship between the transmitted photon rate $I(m)$ and average

received photon count of the SPAD array μ_m can be expressed as

$$\mu_m = \Upsilon [\alpha I(m) + \lambda_{b,\text{tot}}] T_s e^{-\frac{\Upsilon [\alpha I(m) + \lambda_{b,\text{tot}}] T_d}{N}}, \quad (27)$$

To ensure that the distortion induced by SPAD receiver can be compensated, $I(m)$ in the proposed system, denoted as $I_{\text{pre}}(m)$, should be designed so that the received PAM signals are equidistant, i.e.,

$$\mu_{\text{pre},m} = m d_{\text{pre}} + \xi_{\text{pre}}, \quad (28)$$

where d_{pre} denotes the PAM level separation of the SPAD output and ξ_{pre} is a constant value. By substituting (28) into (27), the desired transmitted photon rate is given by

$$I_{\text{pre}}(m) = \frac{-N \mathcal{W}_0 \left(-\frac{(m d_{\text{pre}} + \xi_{\text{pre}}) T_d}{N T_s} \right)}{\alpha \Upsilon T_d} - \frac{\lambda_{b,\text{tot}}}{\alpha}, \quad (29)$$

where $\mathcal{W}_0(x)$ denotes the principal branch of the Lambert W function. The transmitted photon rate (29), or equivalently the pre-distortion transform, should satisfy the constraints (10), (11) and (13) mentioned in Section II-A.

By substituting (29) into (10) and after some mathematical manipulations, the constant ξ_{pre} can be expressed as

$$\xi_{\text{pre}} = \lambda_{b,\text{tot}} \Upsilon T_s e^{-\frac{\lambda_{b,\text{tot}} \Upsilon T_d}{N}}. \quad (30)$$

In addition, the peak power constraint (13) can be rewritten as

$$d_{\text{pre}} \leq \frac{\frac{N T_s}{e T_d} - \xi_{\text{pre}}}{M - 1} = d_{\text{pre},\text{max}}. \quad (31)$$

Substituting (29) into (11), the average power constraint can be expressed as

$$\underbrace{\frac{1}{M} \sum_{m=0}^{M-1} \mathcal{W}_0 \left(-\frac{(m d_{\text{pre}} + \xi_{\text{pre}}) T_d}{N T_s} \right)}_{\mathcal{L}(d_{\text{pre}})} \geq \frac{-\Upsilon T_d}{N h \nu} (\alpha P_{\text{ave}} + \lambda_{b,\text{tot}} h \nu), \quad (32)$$

where $\mathcal{L}(d_{\text{pre}})$ refers to the function at the left hand side of (32). As $\mathcal{W}_0(x)$ is a monotonically increasing function for $x \in [-1/e, 0]$, $\mathcal{L}(d_{\text{pre}})$ is a monotonically decreasing function with

respect to d_{pre} with the maximal value

$$\mathcal{L}(0) = \mathcal{W}_0 \left(\frac{-\lambda_{b,\text{tot}} \Upsilon T_d}{N} e^{\frac{-\lambda_{b,\text{tot}} \Upsilon T_d}{N}} \right) = \frac{-\lambda_{b,\text{tot}} \Upsilon T_d}{N}. \quad (33)$$

and the minimal value $\mathcal{L}(d_{\text{pre},\text{max}})$. Therefore, the inequality (32) can be expressed as $d_{\text{pre}} \leq d_{\text{pre},\text{root}}$ when $\mathcal{L}(d_{\text{pre},\text{max}}) \leq \frac{-\Upsilon T_d}{Nh\nu} (\alpha P_{\text{ave}} + \lambda_{b,\text{tot}} h\nu)$ is satisfied and $d_{\text{pre}} \leq d_{\text{pre},\text{max}}$ otherwise, where $d_{\text{pre},\text{root}}$ denotes the single positive root of (32) when the equality holds which can be calculated numerically through the bisection method. As larger d_{pre} indicates better BER performance, the optimal d_{pre} , denoted as d_{pre}^* , can hence be expressed as

$$d_{\text{pre}}^* = \begin{cases} d_{\text{pre},\text{root}}, & \mathcal{L}(d_{\text{pre},\text{max}}) \leq \frac{-\Upsilon T_d}{Nh\nu} (\alpha P_{\text{ave}} + \lambda_{b,\text{tot}} h\nu), \\ d_{\text{pre},\text{max}}, & \text{otherwise.} \end{cases} \quad (34)$$

By substituting the derived ξ_{pre} in (30) and d_{pre}^* in (34) into (29), the pre-distortion transform at the transmitter can be determined.

As shown in (28), due to the utilisation of the signal pre-distortion, the constellation levels at the receiver are equidistant with a separation of d_{pre}^* . Substituting (28) into (7) and (9) the variance of the received signal, denoted as $\sigma_{\text{pre},m}^2$, can be determined which is, however, still signal dependent. Therefore, the BER of the considered system is again given by (19) with the optimal decoding thresholds calculated based on the derived moments $\mu_{\text{pre},m}$ and $\sigma_{\text{pre},m}^2$.

B. System with Joint Pre-Distortion and Noise Normalization

As illustrated in Section II-C, the system with SQRT cannot successfully normalize the noise variance of SPAD-based OWC systems due to the nonlinear relationship between the noise variance and signal amplitude. In this section, we aim to design a novel SPAD-based OWC system with joint pre-distortion and noise normalization functionality. The schematic of the proposed system is demonstrated in Fig. 2. Different from the system discussed in Section III-A, in this system an additional variance normalizing transform (VNT) and inverse VNT are employed at the receiver and transmitter, respectively. The proposed system can not only achieve the equidistant PAM signals at the receiver as the system considered in Section III-A, but also successfully normalize the noise variance so that the noise becomes signal independent. Thanks to the joint functionality, it is expected that the proposed system outperforms the system

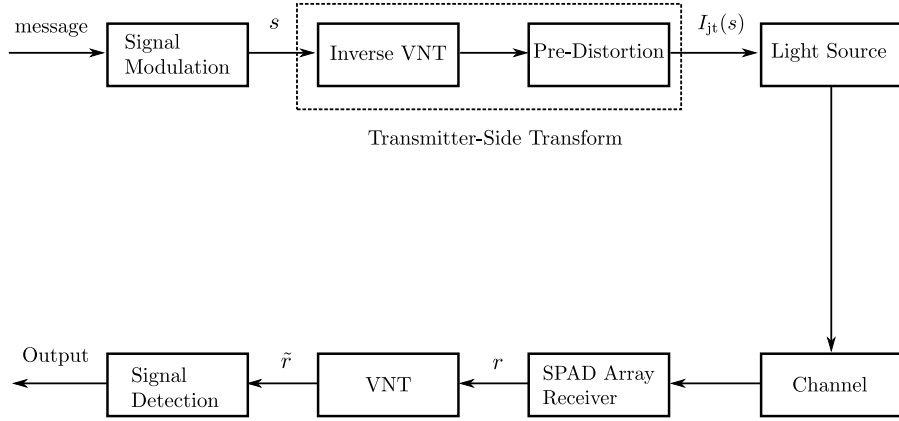


Fig. 2. The schematic of the proposed SPAD-based OWC system with joint pre-distortion and noise normalization.

with only pre-distortion; however, the latter benefits from its simplicity as it does not require any additional signal processing at the receiver. In the following discussion, the design of the transformations involved in the proposed system will be investigated.

The variance of the output of SPAD pixel given in (7) can be further simplified as

$$\sigma_{m,\text{single}}^2 = \mu_{m,\text{single}} - \mu_{m,\text{single}}^2 \vartheta, \quad (35)$$

where

$$\vartheta = 1 - \left[\left(1 - \frac{T_d}{T_s} \right)^+ \right]^2, \quad (36)$$

with $(x)^+ = \max\{x, 0\}$ and $\vartheta \in (0, 1]$. Denoting the output signal of SPAD array receiver as r , as mentioned in Section II-A it is approximately Gaussian distributed. Invoking (9) the variance of r can be expressed as

$$\sigma_m^2 = \mu_m - \frac{\vartheta}{N} \mu_m^2. \quad (37)$$

Let's firstly consider the design of VNT at the receiver. The VNT is applied to random variables with certain relationships between the variance and mean to generate approximately Gaussian random variables with variance independent of the mean [13], [15], [17], [25]¹. Defining the relationship between the mean and variance of the received SPAD signal given in (37) as $\sigma_m^2 =$

¹Note that the convergence to Gaussian random variables is shown for the random variables with original gamma distribution [25], Gaussian distribution [13], noncentral chi-squared distribution [17], and an unknown distribution [15].

$f^2(\mu_m)$, the function $f(x)$ can be expressed as

$$f(x) = \sqrt{x - \frac{\vartheta}{N}x^2}. \quad (38)$$

The VNT at the receiver aiming to normalize the signal-dependent noise can be expressed as [13]

$$\mathcal{T}(x) = \int \frac{1}{f(x)} dx = \int \frac{1}{\sqrt{x - \frac{\vartheta}{N}x^2}} dx. \quad (39)$$

The above integral can be solved analytically as

$$\mathcal{T}(x) = -\sqrt{\frac{N}{\vartheta}} \arcsin\left(-\frac{2\vartheta}{N}x + 1\right). \quad (40)$$

Denoting the transformed signal after VNT as \tilde{r} , i.e., $\tilde{r} = \mathcal{T}(r)$, it is with mean $\mu_{\tilde{r}} \simeq \mathcal{T}(\mu_m)$ and variance $\sigma_{\tilde{r}}^2 \simeq 1$ when μ_m is relatively high. Note that the noise variance of \tilde{r} is signal independent. As the received signal r is approximately Gaussian distributed, it is possible (with very low probability) that when applying the transformation $\mathcal{T}(r)$, the value $-\frac{2\vartheta}{N}r + 1$ is out of the domain of arcsine function, i.e., $[-1, 1]$. To address this issue, before applying the transformation, we truncate r such that $r = N/\vartheta$ and $r = 0$ when $r > N/\vartheta$ and $r < 0$ are satisfied, respectively.

Now let's turn to the design of the transformation at the transmitter. The PAM signal is transformed into the transmitted photon rate $I_{jt}(m)$ and then propagated through the free-space channel. The objective is that for the received signal after VNT the noise variance is signal independent and the constellation levels are equidistant, i.e.,

$$\tilde{r} = \mu_{\tilde{r}} + n_{\tilde{r}}, \quad (41)$$

with

$$\mu_{\tilde{r}} = md_{jt} + \xi_{jt}, \quad (42)$$

where $n_{\tilde{r}}$ is the approximately Gaussian distributed noise with zero mean and normalized variance equal to one, d_{jt} refers to the PAM level separation after VNT, and ξ_{jt} is a constant value. To achieve this goal, the transmitter side transformation should inverse both VNT and the non-linear distortion caused by SPAD channel. Considering that $\mu_{\tilde{r}} \simeq \mathcal{T}(\mu_m)$, (42) can be rewritten as

$$\mathcal{T}(\mu_m) = md_{jt} + \xi_{jt}. \quad (43)$$

By substituting (27) into (43) and after some mathematical manipulations, one can get

$$\mathcal{R} \left(-\frac{\Upsilon T_d [\alpha I_{jt}(m) + \lambda_{b,tot}]}{N} \right) = \frac{-\mathcal{T}^{-1}(md_{jt} + \xi_{jt})T_d}{NT_s}, \quad (44)$$

where the function $\mathcal{R}(x) = xe^x$ and $\mathcal{T}^{-1}(x)$ denotes the inverse function of $\mathcal{T}(x)$ which can be expressed as

$$\mathcal{T}^{-1}(x) = \frac{-N}{2\vartheta} \left[\sin \left(-\sqrt{\frac{\vartheta}{N}} x \right) - 1 \right]. \quad (45)$$

Equation (44) can be rewritten as

$$\frac{-\Upsilon T_d [\alpha I_{jt}(m) + \lambda_{b,tot}]}{N} = \mathcal{W}_0 \left\{ \frac{-\mathcal{T}^{-1}(md_{jt} + \xi_{jt})T_d}{NT_s} \right\}. \quad (46)$$

Based on (46), the desired transmitted photon rate when the m th symbol is transmitted can be expressed as

$$I_{jt}(m) = \frac{-N\mathcal{W}_0 \left\{ -\frac{T_d}{NT_s} \mathcal{T}^{-1}(md_{jt} + \xi_{jt}) \right\}}{\alpha \Upsilon T_d} - \frac{\lambda_{b,tot}}{\alpha}. \quad (47)$$

This transmitted photon rate, or equivalently the transmitter side transformation, has the similar shape to that of the system with only pre-distortion given in (29). The difference is that in this proposed system, the generated PAM signal firstly goes through an additional inverse VNT which is given by $-\frac{T_d}{NT_s} \mathcal{T}^{-1}(md_{jt} + \xi_{jt})$ after which the pre-distortion transform is applied. Therefore, the transmitter side transform can be divided into two sub-transforms, i.e., inverse VNT and pre-distortion, as illustrated in Fig. 2.

In order to apply the derived transformations at the transmitter, the PAM level separation d_{jt} and the constant ξ_{jt} in (47) should be determined. Substituting (47) into the first considered constraint (10) and after some mathematical manipulations, one can get

$$\xi_{jt} = -\sqrt{\frac{N}{\vartheta}} \arcsin \left(\frac{-2\vartheta T_s \lambda_{b,tot} \Upsilon}{N} e^{-\frac{\lambda_{b,tot} \Upsilon T_d}{N}} + 1 \right).$$

On other hand, the peak power constraint given in (13) can be rewritten as

$$d_{jt} \leq \frac{-\sqrt{\frac{N}{\vartheta}} \arcsin \left(-\frac{2\vartheta T_s}{T_d e} + 1 \right) - \xi_{jt}}{M - 1} = d_{jt,\max}. \quad (48)$$

It can be easily shown that $\vartheta T_s / T_d e \in (0, \frac{1}{e}]$ when $T_d \geq T_s$ and $\vartheta T_s / T_d e \in (\frac{1}{e}, \frac{2}{e})$ when $T_d < T_s$. Therefore, in both cases, the term $-2\vartheta T_s / T_d e + 1$ in (48) is within the domain of the arcsine

function for real results. Finally, with the expression of $I_{jt}(m)$ given in (47), the average power constraint (11) can be expressed as

$$\underbrace{\frac{1}{M} \sum_{m=0}^{M-1} \mathcal{W}_0 \left\{ \frac{T_d}{2\vartheta T_s} \left[\sin \left(-\sqrt{\frac{\vartheta}{N}} (md_{jt} + \xi_{jt}) \right) - 1 \right] \right\}}_{\mathcal{L}'(d_{jt})} \geq \frac{-\Upsilon T_d}{Nh\nu} (\alpha P_{ave} + \lambda_{b,tot} h\nu). \quad (49)$$

Note that we denote the function at the left hand side of the above inequality as $\mathcal{L}'(d_{jt})$. It can be proven that $\mathcal{L}'(d_{jt})$ is a monotonically decreasing function with respect to d_{jt} with the maximal value

$$\mathcal{L}'(0) = \mathcal{W}_0 \left(\frac{T_d}{2\vartheta T_s} \left[\sin \left(-\sqrt{\frac{\vartheta}{N}} \xi_{jt} \right) - 1 \right] \right) = \frac{-\lambda_{b,tot} \Upsilon T_d}{N}. \quad (50)$$

Invoking the constraint (48), the minimal value of $\mathcal{L}'(d_{jt})$ is $\mathcal{L}'(d_{jt,max})$. Using the same method employed to derive the optimal d_{pre} given in (34), the optimal d_{jt} , denoted as d_{jt}^* , can be expressed as

$$d_{jt}^* = \begin{cases} d_{jt,root}, & \mathcal{L}'(d_{jt,max}) \leq \frac{-\Upsilon T_d}{Nh\nu} (\alpha P_{ave} + \lambda_{b,tot} h\nu), \\ d_{jt,max}, & \text{otherwise.} \end{cases} \quad (51)$$

where $d_{jt,root}$ denotes the single positive root of (49) when the equality holds which can be achieved numerically. Substituting the derived ξ_{jt} in (48) and d_{jt}^* in (51) into (47), the transformations at the transmitter can be determined.

By utilizing the transformations at transmitter and receiver given by (47) and (40), respectively, the proposed system has joint pre-distortion and noise normalization functionality. Assuming that the noise normalization process is ideal, the transformed signal at the receiver is Gaussian distributed with signal independent noise. In addition, thanks to the signal pre-distortion, its constellation levels are equally spaced with distance d_{jt}^* . In effect, the conventional signal detection techniques designed for AWGN channel can be performed to the transformed signal to recover the original message. Therefore the BER of the proposed system can be expressed as the BER for PAM modulation in AWGN channel given by

$$P_{eb,jt} \approx \frac{2M-2}{M \log_2(M)} Q \left(\frac{d_{jt}^*}{2\sigma_r} \right) = \frac{2M-2}{M \log_2(M)} Q \left(\frac{d_{jt}^*}{2} \right). \quad (52)$$

It is worth noting that after the VNT at the receiver, the signal distribution is not exactly Gaussian,

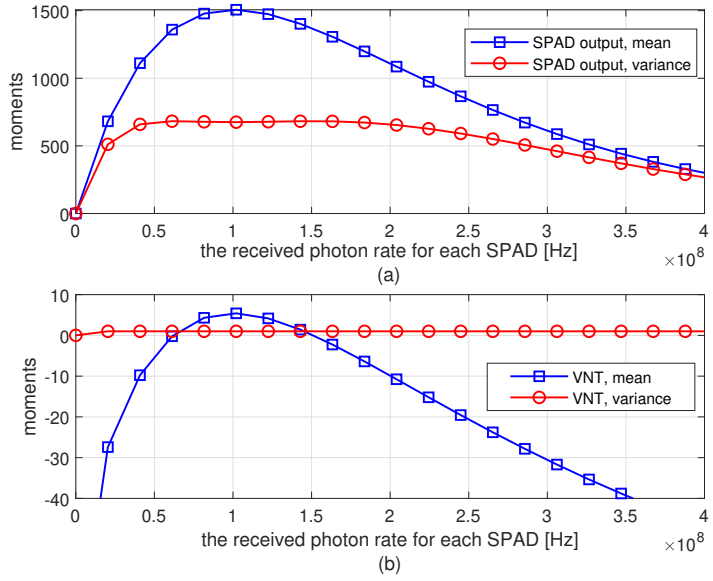


Fig. 3. The mean and variance of (a) the original SPAD output signal and (b) the signal after the proposed VNT at the receiver (40). The symbol duration is $T_s = 20$ ns.

hence the given BER expression (52) is an approximation. Later in Section IV, it is demonstrated that this analytical BER only slightly outperforms the exact BER performance achieved through simulation, which indicates that (52) is a good approximation.

IV. NUMERICAL RESULTS

In this section, we present some simulation results to show the advantages of the proposed SPAD-based OWC systems in Section III over the state-of-the-art systems introduced in Section II. The SPAD array employed in these systems is assumed to be with 2048 SPAD pixels, the PDE is $\Upsilon = 0.18$, the dead time T_d is set as 10 ns [26], the optical wavelength is $\lambda = 785$ nm, and the path loss coefficient is $\alpha = -30$ dB [27]. We consider 4-PAM as the modulation scheme, although other PAM modulation schemes can also be employed which can result in similar conclusions.

Firstly, let's consider the effectiveness of the VNT given in (40). Fig. 3 shows the mean and variance of the original SPAD output signal and the signal after the VNT versus the received photon rate. As shown in Fig. 3(a), the noise variance of SPAD output is signal dependent and is less than the mean value which reveals the sub-Poisson characteristics of the SPAD signal.

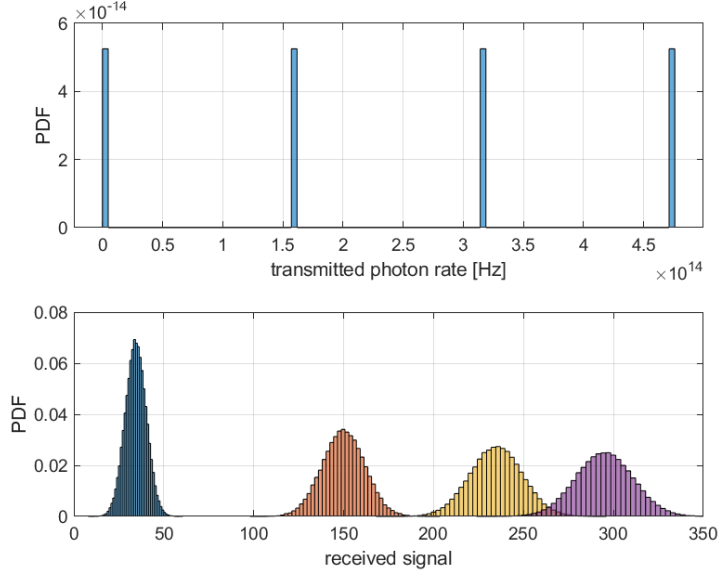


Fig. 4. The signal PDFs of the system with uniform signalling when the transmitted optical power is $60 \mu\text{W}$, the received background power is $P_b = 10 \text{ nW}$, and symbol duration is $T_s = 5 \text{ ns}$.

However, when the VNT is applied, as demonstrated in Fig. 3(b), with the increase of received photon rate the noise variance of the transformed signal quickly increases to 1 and becomes fixed at this value. Therefore, the variance of the noise can be successfully normalized by employing the designed VNT at the receiver.

Figure 4 presents an example of the PDFs of the transmitted photon rate and the corresponding received signal for the system with uniform signalling. It is shown that even though the transmitted photon rates are uniformly spaced, due to the SPAD-induced non-linear distortion and shot noise effects, the received signal levels are not uniformly spaced and the signal variance is strongly signal dependent. For instance, the distance between the first two received constellation levels is around 115; however, the distance between the last two levels is only 60. In addition, the variance of the received signal when the lowest level is transmitted is 34; whereas, the corresponding variance when the highest level is transmitted increases to 252.

Figure 5 demonstrates the signal PDFs of the proposed system with pre-distortion. It is shown that with the employed signal pre-distortion at the transmitter, the received constellation levels successfully become equidistant with a separation of 93. However, the noise is still signal-dependent and higher signal level still results in higher noise variance. On the other hand, Fig.

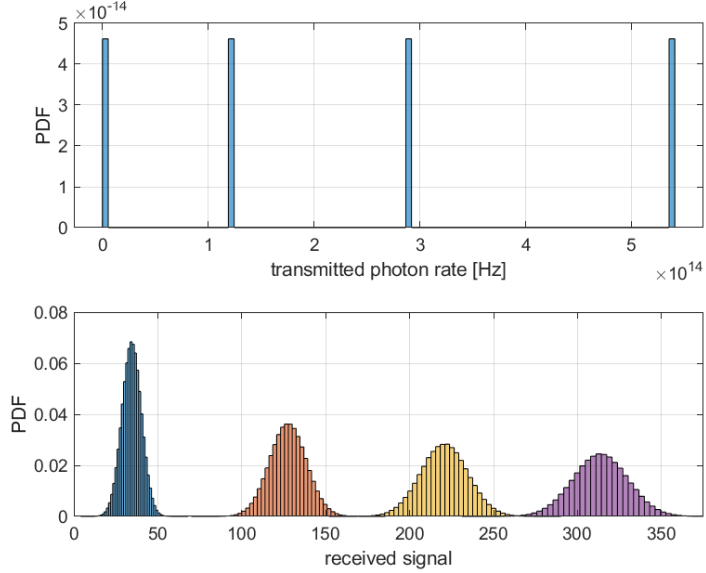


Fig. 5. The signal PDFs of the proposed system with signal pre-distortion when transmitted optical power is $60 \mu\text{W}$, the received background power is $P_b = 10 \text{ nW}$, and symbol duration is $T_s = 5 \text{ ns}$.

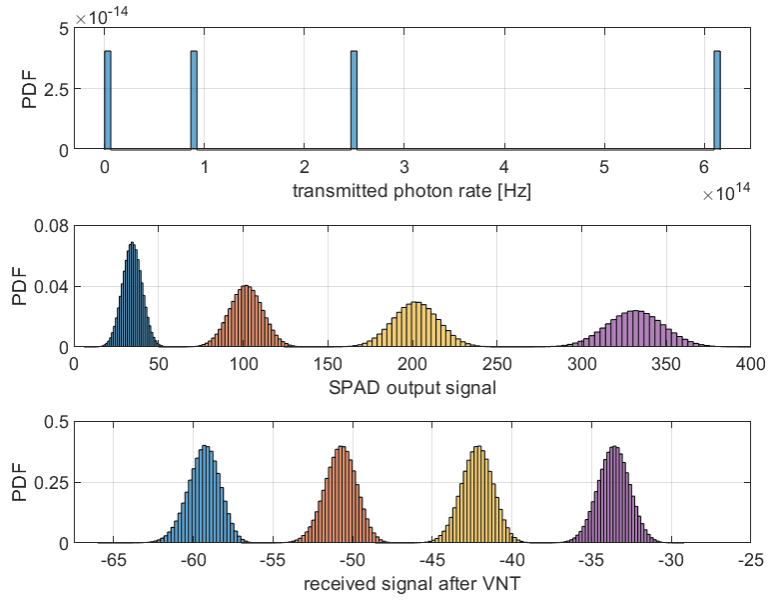


Fig. 6. The signal PDFs of the proposed system with joint functionality when transmitted optical power is $60 \mu\text{W}$, the received background power is $P_b = 10 \text{ nW}$, and symbol duration is $T_s = 5 \text{ ns}$.

6 presents the PDFs of the signals for the proposed system with joint pre-distortion and noise

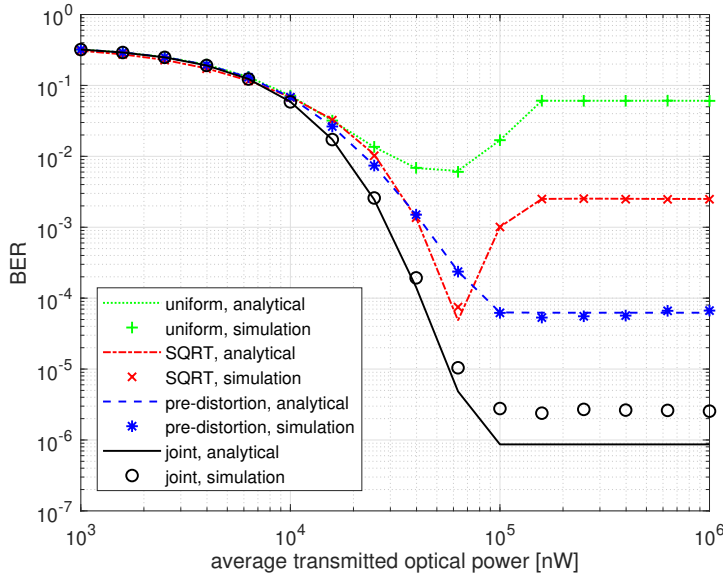


Fig. 7. The BER versus the average transmitted optical power for systems with different schemes when the symbol duration is $T_s = 5$ ns and the received background power is $P_b = 10$ nW.

normalization functionality. One can observe that, similar to system with only pre-distortion, the constellation levels of the signal after the VNT are also equally spaced (with distance 8.6). However, the difference is that for such system the noise variances when different signal levels are transmitted are also identical (approximately equal to 1) hence the noise is signal independent. Therefore, in this considered system both the non-linear distortion and signal-dependent noise of the SPAD output are eliminated as expected.

Figure 7 and Figure 8 present the BER versus the average transmitted optical power for the investigated systems under two different background power levels. For the system with uniform signalling, with the increase of the transmitted power, the BER firstly decreases and then increases due to the non-linear distortion effects of the SPAD. With further increase of the transmitted power, the BER saturates at a fixed value. This is because of the considered peak power constraint (13) which results in the BER performance becomes average power independent in high average power regime. The same BER saturation effect can also be observed in the other systems. The system with SQRT performs slightly better than that with uniform signalling but they are with similar BER shapes. On the other hand, for the proposed systems, i.e., systems with pre-distortion and joint functionality, thanks to the signal pre-distortion which compensates the SPAD non-

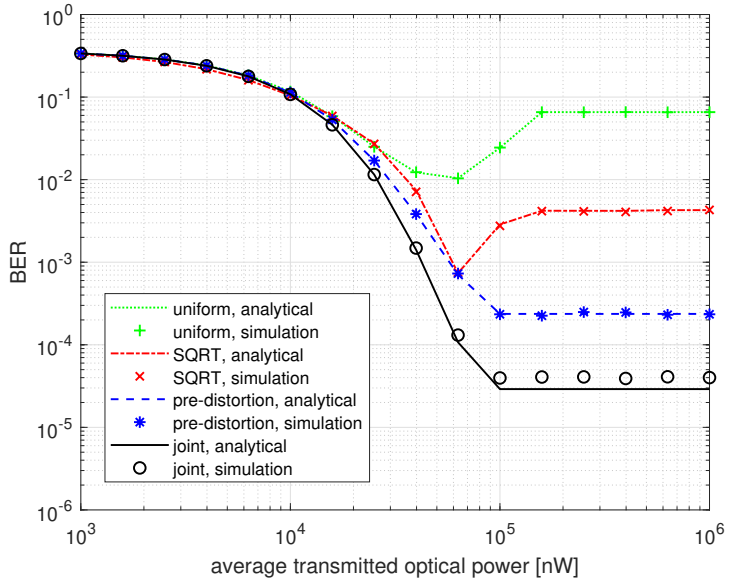


Fig. 8. The BER versus the average transmitted optical power for systems with different schemes when the symbol duration is $T_s = 5$ ns and the received background power is $P_b = 20$ nW.

linear effects at the transmitter, the BER monotonically decreases and then saturates with the increase of the transmitted power. It is demonstrated that generally these two proposed systems can result in much better performance compared to the state-of-the-art systems especially in high power regimes. In addition, the proposed system with joint functionality can achieve the best BER performance over the whole considered optical power regime. For example, when the transmitted optical power is $100 \mu\text{W}$ and the received background power is 10 nW, the BER values of the systems with uniform signalling, SQRT, and pre-distortion are given by 2×10^{-2} , 10^{-3} and 6.2×10^{-5} , respectively. However, the corresponding BER of the proposed system is only 2.7×10^{-6} . It is shown in these two figures that for the considered systems except the one with joint functionality, the analytical results exactly match with the simulation ones, which justifies our analytical derivations. For the system with joint functionality, the analytical result slightly outperforms the simulation result. This is because after the VNT at the receiver, the transformed signal is not exactly Gaussian distributed. As a result, the analytical BER expression given in (52) which is calculated based on the ideal Gaussian distributed signal cannot perfectly match the corresponding simulation result. However, the small deviation between the analytical and simulation result indicates that this analytical expression is still a good approximation of

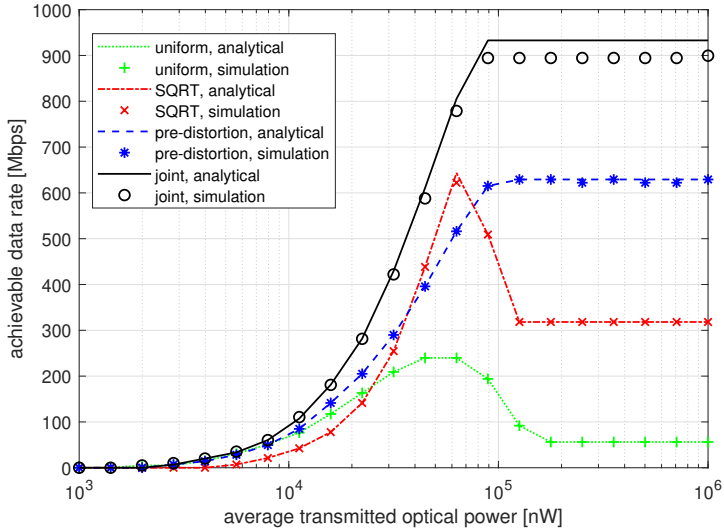


Fig. 9. The achievable data rate versus the average transmitted power for different schemes when the BER target is 10^{-3} and the received background power is $P_b = 10$ nW.

the simulation result.

By comparing Fig. 7 and Fig. 8, it is presented that the increase of the received background power can result in significant BER degradation to all of the considered systems. In addition, higher background power also leads to the reduction of the performance gap between the system with joint functionality and the system with only pre-distortion. This is because higher background power introduces less available dynamic range and results in the less difference among the variances when different signal levels are transmitted. Consequently, for the system with joint functionality, the performance improvement induced by additional noise normalization reduces, which makes its performance closer to that of the system with only pre-distortion.

Finally, in order to provide some insights on the improvement of achievable data rate by using the proposed systems, the achievable data rates versus the average transmitted power for different systems are plotted in Fig. 9. In the simulation, a target BER of 10^{-3} is employed and for each given transmitted optical power the maximum data rate of the considered system satisfying the BER target is recorded. It is clearly demonstrated that generally the proposed systems can effectively improve the achievable data rate. In particular, the proposed system with joint functionality can achieve the highest data rate over the considered range of optical power. For instance, when the transmitted optical power is $200 \mu\text{W}$, the achievable data rate of the

proposed system with joint functionality is 900 Mbps; however, the corresponding data rates for system with uniform signalling, SQRT and pre-distortion are only 56 Mbps, 318 Mbps and 630 Mbps, respectively.

V. CONCLUSION

The performance of the SPAD-based OWC systems is strongly degraded by dead-time-induced non-linear distortion and signal dependent noise. To mitigate the dead time effects and improve the communication performance, two novel systems are proposed in this work which can be easily implemented without additional hardware requirements. By comparing the proposed systems with the state-of-the-art systems, it is demonstrated that the proposed systems can significantly improve the BER performance and achievable data rate and enhance the tolerance of the background power. In particular, it is demonstrated that when the background power is 10 nW, with a target BER of 10^{-3} the proposed two systems can achieve data rates of 630 Mbps and 900 Mbps; whereas, the corresponding data rates for state-of-the-art systems are below 320 Mbps.

VI. ACKNOWLEDGEMENTS

We gratefully acknowledge the financial support from EPSRC under grant EP/R023123/1 (ARROW).

REFERENCES

- [1] D. Chitnis and S. Collins, “A SPAD-based photon detecting system for optical communications,” *J. Lightwave Technol.*, vol. 32, no. 10, pp. 2028–2034, May 2014.
- [2] Y. Li, M. Safari, R. Henderson, and H. Haas, “Optical OFDM with single-photon avalanche diode,” *IEEE Photonics Technology Letters*, vol. 27, no. 9, pp. 943–946, May 2015.
- [3] M. Khalighi, T. Hamza, S. Bourennane, P. Léon, and J. Opderbecke, “Underwater wireless optical communications using silicon photo-multipliers,” *IEEE Photonics Journal*, vol. 9, no. 4, pp. 1–10, 2017.
- [4] S. Huang, S. M. Patanwala, J. Kosman, R. K. Henderson, and M. Safari, “Optimal photon counting receiver for sub-dead-time signal transmission,” *Journal of Lightwave Technology*, vol. 38, no. 18, pp. 5225–5235, 2020.
- [5] H. Zimmermann, “APD and SPAD receivers : Invited paper,” in *2019 15th International Conference on Telecommunications (ConTEL)*, 2019, pp. 1–5.
- [6] E. Fisher, I. Underwood, and R. Henderson, “A reconfigurable single-photon-counting integrating receiver for optical communications,” *IEEE Journal of Solid-State Circuits*, vol. 48, no. 7, pp. 1638–1650, July 2013.
- [7] L. Zhang, D. Chitnis, H. Chun, S. Rajbhandari, G. Faulkner, D. O’Brien, and S. Collins, “A comparison of APD- and SPAD-based receivers for visible light communications,” *J. Lightwave Technol.*, vol. 36, no. 12, pp. 2435–2442, Jun 2018.

- [8] Z. Ahmed, R. Singh, W. Ali, G. Faulkner, D. O'Brien, and S. Collins, "A SiPM-based VLC receiver for Gigabit communication using OOK modulation," *IEEE Photonics Technology Letters*, vol. 32, no. 6, pp. 317–320, 2020.
- [9] M. A. Khalighi, H. Akhouayri, and S. Hranilovic, "Silicon-photomultiplier-based underwater wireless optical communication using pulse-amplitude modulation," *IEEE Journal of Oceanic Engineering*, pp. 1–11, 2019.
- [10] S. Huang and M. Safari, "Hybrid SPAD/PD receiver for reliable free-space optical communication," *IEEE Open Journal of the Communications Society*, vol. 1, pp. 1364–1373, 2020.
- [11] M. Karbalayghareh, F. Miramirkhani, M. Safari, and M. Uysal, "Vehicular visible light communications with SPAD receivers," in *2019 IEEE Wireless Communications and Networking Conference (WCNC)*, 2019, pp. 1–5.
- [12] S. Cova, M. Ghioni, A. Lacaita, C. Samori, and F. Zappa, "Avalanche photodiodes and quenching circuits for single-photon detection," *Appl. Opt.*, vol. 35, no. 12, pp. 1956–1976, Apr 1996.
- [13] M. Safari, "Efficient optical wireless communication in the presence of signal-dependent noise," in *2015 IEEE International Conference on Communication Workshop (ICCW)*, 2015, pp. 1387–1391.
- [14] Q. Gao, S. Hu, C. Gong, and Z. Xu, "Modulation designs for visible light communications with signal-dependent noise," *J. Lightwave Technol.*, vol. 34, no. 23, pp. 5516–5525, Dec 2016.
- [15] I. Tavakkolnia and M. Safari, "Capacity analysis of signaling on the continuous spectrum of nonlinear optical fibers," *Journal of Lightwave Technology*, vol. 35, no. 11, pp. 2086–2097, 2017.
- [16] I. Tavakkolnia and M. Safari, "Signaling on the continuous spectrum of nonlinear optical fiber," *Opt. Express*, vol. 25, no. 16, pp. 18 685–18 702, Aug 2017.
- [17] Y. Chen, I. T. A. Alvarado, and M. Safari, "On the capacity of amplitude modulated soliton communication over long haul fibers," *Entropy*, vol. 22, no. 8, p. 899, Aug 2020.
- [18] E. Sarbazi, M. Safari, and H. Haas, "Statistical modeling of single-photon avalanche diode receivers for optical wireless communications," *IEEE Transactions on Communications*, vol. 66, no. 9, pp. 4043–4058, Sep. 2018.
- [19] K. Omote, "Dead-time effects in photon counting distributions," *Nuclear Instruments and Methods in Physics Research Section A: Accelerators, Spectrometers, Detectors and Associated Equipment*, vol. 293, no. 3, pp. 582–588, 1990.
- [20] A. Eisele, R. Henderson, B. Schmidtke, T. Funk, L. Grant, J. Richardson, and W. Freude, "185 MHz count rate 139 dB dynamic range single-photon avalanche diode with active quenching circuit in 130 nm CMOS technology," in *Proc. Int. Image Sensor Workshop*, 2011, pp. 278–280.
- [21] D. Zou, C. Gong, K. Wang, and Z. Xu, "Characterization on practical photon counting receiver in optical scattering communication," *IEEE Transactions on Communications*, vol. 67, no. 3, pp. 2203–2217, 2019.
- [22] F. Y. Daniel and J. A. Fessler, "Mean and variance of single photon counting with deadtime," *Physics in Medicine & Biology*, vol. 45, no. 7, p. 2043, 2000.
- [23] ON Semiconductor, "J-SERIES SIPM: Silicon photomultiplier sensors, J-Series (SiPM)," Accessed: Dec 11, 2020. [Online]. Available: <https://www.onsemi.com/products/sensors/silicon-photomultipliers-sipm/j-series-sipm>.
- [24] H. Elgala, R. Mesleh, and H. Haas, "Non-linearity effects and predistortion in optical OFDM wireless transmission using LEDs," *International Journal of Ultra Wideband Communications and Systems*, vol. 1, no. 2, pp. 143–150, 2009.
- [25] P. R. Prucnal and B. E. A. Saleh, "Transformation of image-signal-dependent noise into image-signal-independent noise," *Opt. Lett.*, vol. 6, no. 7, pp. 316–318, Jul 1981.
- [26] S. M. Patanwala, I. Gyongy, N. A. Dutton, B. R. Rae, and R. K. Henderson, "A reconfigurable 40 nm CMOS SPAD array for LiDAR receiver validation," in *2019 International Image Sensor Workshop*.
- [27] I. I. Kim, J. Koontz, H. Hakakha, P. Adhikari, and *et al.*, "Measurement of scintillation and link margin for the TerraLink

laser communication system," in *Wireless Technologies and Systems: Millimeter-Wave and Optical*, vol. 3232, 1998, pp. 100 – 118.